We are IntechOpen, the world's leading publisher of Open Access books Built by scientists, for scientists

4,800
Open access books available

122,000
International authors and editors

135M
Downloads

Our authors are among the

154
Countries delivered to

TOP 1%
most cited scientists

12.2%
Contributors from top 500 universities

CLARIVATE ANALYTICS BOOK CITATION INDEX INDEXED

WEB OF SCIENCE™

Selection of our books indexed in the Book Citation Index in Web of Science™ Core Collection (BKCI)

Interested in publishing with us?
Contact book.department@intechopen.com

Numbers displayed above are based on latest data collected.
For more information visit www.intechopen.com

3

Combined Torque and Velocity Control of a Redundant Robot System

Damir Omrčen, Leon Žlajpah, Bojan Nemec
Jožef Stefan Institute
Slovenia

1. Introduction

One of the most important features of the next generation of robots is the mobility and the ability to work in an unstructured environment. Conventional manipulator arms have bounded workspace and are thus appropriate only for some limited tasks. Hence, they need additional devices such as conveyor belts and handling devices in order to perform a task requiring large workspace. A new promising concept is to place a manipulator arm on a mobile platform. Such system is usually called mobile manipulator. This adds extra degrees of freedom to the system, which makes the mobile manipulator more dexterous and it may become redundant. Redundancy is an important feature of the new generation of robots making them more versatile. For example, a redundant robot can avoid obstacles in the workspace while executing given task or it can optimize joint torques without modifying primary task, which is usually position and/or force tracking of the robot tool mounted on the top of the robot arm.

Mobile manipulators typically consist of a robot manipulator mounted on a mobile platform. Typically, the workspace of the fixed base manipulators is limited but they have good accuracy and fast dynamics. On the contrary, mobile platforms have an "infinite" workspace but they are slow and inaccurate, they can not perform any task by itself. Integration of a fast and accurate manipulator and a platform results in a mobile manipulator that should integrate good properties of both subsystems. Hence, the mobile manipulator has large workspace and high dynamics. Its accuracy is comparable to the fixed manipulator accuracy using appropriate sensors and appropriate control algorithm.

Due to the remarkable properties mobile manipulators are often used as service robots that help humans in everyday jobs in everyday environments. When working in unknown environment robot autonomy is crucial. The key feature to assure autonomy is the obstacle avoidance. Therefore, appropriate sensors are needed.

Compliant behavior is essential when a robot is in contact with the environment (Asada and Slotine [1986]), e.g. in robot assembling, grinding, driving a screw etc. The usual approaches to compliant motion control are the impedance control (Hogan [1985], Salisbury [1980]), the dynamic hybrid control (Raibert and Craig [1981]) and the (resolved) acceleration control (Luh et al. [1980]). The impedance control does not control forces or positions directly, but it controls the desired dynamics of the end-effector or its stiffness. When the dynamic hybrid control is used, the position is controlled along selected directions, while forces are

Source: Mobile Robots, Moving Intelligence, ISBN: 3-86611-284-X, Edited by Jonas Buchli, pp. 576, ARS/plV, Germany, December 2006

controlled along the others directions. Using the resolved acceleration control the force is not controlled directly although we can achieve compliant behavior. The goal of our research is to develop appropriate control algorithm that enables compliant motion of a redundant mobile manipulator in unstructured environments.

A lot of research has been done recently on the control of mobile manipulators (Khatib [1999], Yamamoto and Yun [1996], Altafini [2001], Petersson et al. [2000], Oropeza and Devy [1999], Omrčen et. al. [2004]). Regarding control signals there are two basic types of robot control: velocity and torque control. In the case of a velocity control the control signals are velocities in the robot joints and in the other case control signals are joint torques. Generally, from the performance point of view the torque control has a lot of advantages over the velocity control. However, the torque control can be used only if the robot is equipped with a corresponding motor controller. In fact, most commercially available mobile platforms are velocity controlled and on the other hand manipulators usually enable torque or velocity control. To solve the control problem usually the velocity control is used for both subsystems (a manipulator and a platform). This choice could result in decreased performances of the overall system. To overcome this problem a modification of the motor controller hardware is possible (Holmberg and Khatib [2000]). This is expensive and requires a lot of development. To preserve the advantages of the torque control, while using the existing velocity motor controller, we propose to use a *combined control* ((Omrčen et al. [2004])) where the velocity and the torque control are combined in a single control system.

We have examined the combined control in details analytically and experimentally on a real and a simulated system. The analysis includes tracking the trajectory reference in the task and null space is shown. Furthermore, the influence of disturbing external forces in the task and null space on the motion of the robot system is also analyzed. Similar analysis for a redundant torque controlled system has been done by Žlajpah (Žlajpah [1999]). He examined in details the influence of the external forces in task and null space in different configurations.

Khatib (Khatib [1995]) proved that a redundant robotic system is dynamically consistent in case of inertia weighted generalized inverse. This is true only for complete torque controlled systems. In case of combined controlled system this is not a case. We will show later, that such system can also be dynamically consistent while using other weight. In this case the system is partly decomposed, which is not desired.

We will show on a real system that using appropriate controller gains we can achieve high compliance of the robot system in the null space and high stiffness in the task space. This enables obstacle avoidance without use of any sensors and successful trajectory tracking. Since the robot is redundant, the obstacle avoidance can be done simultaneously with the primary task. Compliance is also an important property when the robot works in the contact with the environment. We have shown that using combined control we could maintain most of good properties of complete torque control without modification of the controller in the velocity controlled subsystem.

2 Methods

2.1 Mobile manipulator

The mobile manipulator that we used (Fig. 1), consist of a torque controlled planar manipulator with four DOF mounted on a velocity controlled holonomic platform Nomad XR4000 with three DOF. The complete system has seven DOF (n = 7). The task was defined as a positioning in (x-y) plane. So, the task has two DOF (m = 2) and consequently, the

degree of redundancy is five (r = 5). The planar manipulator is back-drivable and it was primary designed to be back-drivable and high speed and we sacrificed the accuracy.
In general, advanced force and trajectory control relies on controlling motors torques directly. Unfortunately, mobile platform which we used enables only position and velocity control. Having in mind this limitation, we propose a combination of velocity controlled platform and torque controlled manipulator.

Fig. 1. Mobile manipulator.

Fist we have to set the mathematical model of the mobile manipulator. Using the Lagrangean formulation, we can express the dynamic model of the complete system in the form

$$\mathbf{H}(\mathbf{q})\ddot{\mathbf{q}} + \mathbf{C}(\dot{\mathbf{q}},\mathbf{q})\dot{\mathbf{q}} + \mathbf{g}(\mathbf{q}) = \tau, \tag{1}$$

here, **H**, **C** in **g** denote the inertia matrix, the vector of Coriolis and centrifugal forces and the vector of gravity forces, respectively. τ is the vector of joint torques and **q** is the vector of joint positions. As one part of the system is controlled by torque and the other part by velocity, the dynamic model (1) is decomposed into

$$\begin{bmatrix} \mathbf{H}_v(\mathbf{q}) & \mathbf{H}_{vt}(\mathbf{q}) \\ \mathbf{H}_{tv}(\mathbf{q}) & \mathbf{H}_t(\mathbf{q}) \end{bmatrix} \begin{bmatrix} \ddot{\mathbf{q}}_v \\ \ddot{\mathbf{q}}_t \end{bmatrix} + \begin{bmatrix} \mathbf{C}_v(\dot{\mathbf{q}},\mathbf{q}) & \mathbf{C}_{vt}(\dot{\mathbf{q}},\mathbf{q}) \\ \mathbf{C}_{tv}(\dot{\mathbf{q}},\mathbf{q}) & \mathbf{C}_t(\dot{\mathbf{q}},\mathbf{q}) \end{bmatrix} \begin{bmatrix} \dot{\mathbf{q}}_v \\ \dot{\mathbf{q}}_t \end{bmatrix} + \begin{bmatrix} \mathbf{g}_v(\mathbf{q}) \\ \mathbf{g}_t(\mathbf{q}) \end{bmatrix} = \begin{bmatrix} \tau_v \\ \tau_t \end{bmatrix}, \tag{2}$$

where $()_v$ indicates the velocity controlled subsystem (platform) and $()_t$ the torque controlled subsystem (manipulator). We assume that the velocity controlled subsystem is lower in kinematic chain and the torque controlled subsystem is higher. This is true for most of the combined controlled system e.g. most mobile manipulators. In other cases the controller can be easily modified.
Since the subsystems are physically connected, the dynamic interaction between both subsystem exist and it is included in $\mathbf{H}_{tv}$, $\mathbf{H}_{vt}$, $\mathbf{H}_v$, $\mathbf{C}_v$,...

2.2 Combined control of the mobile manipulator

The combined control is based on acceleration control (Luh et al. [1980], Hsu et al. [1989]):

$$\tau_c = \hat{\mathbf{H}}(\mathbf{q})\ddot{\mathbf{q}}_c + \hat{\mathbf{C}}(\dot{\mathbf{q}},\mathbf{q})\dot{\mathbf{q}} + \hat{\mathbf{g}}(\mathbf{q}), \tag{3}$$

$$\ddot{\mathbf{q}}_c = \mathbf{J}^{\#}(\ddot{\mathbf{x}}_c - \dot{\mathbf{J}}\dot{\mathbf{q}}) + \mathbf{N}(\Phi - \dot{\mathbf{N}}\dot{\mathbf{q}}), \tag{4}$$

here the motion in the task space and in the null space can be controlled independently. τ_c is the control torque and $\ddot{\mathbf{q}}_c$ is the control acceleration. $(\hat{\cdot})$ indicates the approximation of dynamic model matrices (1). $\mathbf{J}^{\#}$ and $\mathbf{N}^T$ are the generalized inverse of the end-effector Jacobian matrix $\mathbf{J}$ and the projection into the null space of $\mathbf{J}^T$, respectively, and are defined by

$$\mathbf{J}^{\#} = \mathbf{W}^{-1}\mathbf{J}^T(\mathbf{J}\mathbf{W}^{-1}\mathbf{J}^T)^{-1}, \tag{5}$$

$$\mathbf{N} = \mathbf{I} - \mathbf{J}^{\#}\mathbf{J}. \tag{6}$$

Here $\mathbf{W}$ is the generalized inverse weight. $\ddot{\mathbf{x}}_c$ and Φ in Eq. (4) represent the task space and null space control law, respectively, and are defined by:

$$\ddot{\mathbf{x}}_c = \ddot{\mathbf{r}} + \mathbf{K}_d\dot{e} + \mathbf{K}_p e, \quad e = \mathbf{r} - \mathbf{x}, \tag{7}$$

$$\Phi = \mathbf{N}\ddot{\varphi} + \dot{\mathbf{N}}\dot{\varphi} + \mathbf{K}_\mathbf{n}\dot{\mathbf{e}}_\mathbf{n}, \quad \dot{\mathbf{e}}_\mathbf{n} = \mathbf{N}(\dot{\varphi} - \dot{\mathbf{q}}), \tag{8}$$

where **e** is the task space tracking error, *X* and **r** are the actual and the desired task space position, respectively. $\dot{\varphi}$ is the desired null space velocity. K_d and K_p are constant gain matrices that define the task space impedance and K_n is a constant gain matrix that defines the null space damping.

We assume that the torques of the first subsystem in kinematic chain can not be controlled, since the subsystem is controlled by a velocity controller. Therefore, we can not apply the controller (3) directly. Instead of modifying the velocity motor controller in the platform we propose the following controller, which is shown in Fig. 2:

$$\tau_{v_c} = f(\dot{\mathbf{q}}_{v_c}), \tag{9}$$

$$\tau_{t_c} = \begin{bmatrix}\hat{\mathbf{H}}_{vt}(\mathbf{q}) & \hat{\mathbf{H}}_t(\mathbf{q})\end{bmatrix}\begin{bmatrix}\ddot{\mathbf{q}}_{v_c} \\ \ddot{\mathbf{q}}_{t_c}\end{bmatrix} + \begin{bmatrix}\hat{\mathbf{C}}_{tv}(\dot{\mathbf{q}},\mathbf{q}) & \hat{\mathbf{C}}_t(\dot{\mathbf{q}},\mathbf{q})\end{bmatrix}\begin{bmatrix}\dot{\mathbf{q}}_v \\ \dot{\mathbf{q}}_t\end{bmatrix} + \hat{\mathbf{g}}_t(\mathbf{q}). \tag{10}$$

The control accelerations $\ddot{\mathbf{q}}_c$ are divided into two parts: velocity and torque part (see Fig. 2). To control a velocity controlled subsystem we have integrated control accelerations and obtain control velocities. These control velocities define inner torques in the velocity controlled subsystem τ_{v_c} by an unknown nonlinear function $f(\dot{\mathbf{q}}_{v_c})$. This controller considers only the reference velocity $\dot{\mathbf{q}}_{v_c}$. We can presume that the velocity controlled system ensure tracking the velocity reference.

On the other hand the torques of the torque controlled subsystem τ_{t_c} are defined by the user (10). They are obtained using only corresponding part of the controller (3) and includes only a corresponding part of the dynamic model (2). We can see that the motion of the velocity controlled part is completely compensated.

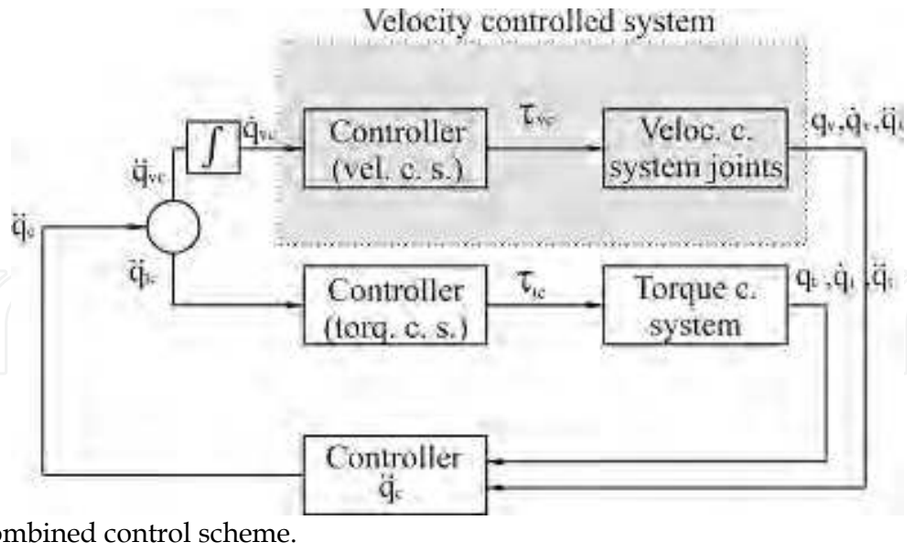

Fig. 2. Combined control scheme.

3. Analysis of the combined controller

This section describes the analysis of the combined control. We examined the trajectory tracking and the influence of the external force.

3.1 Trajectory tracking

One of the basic requirements of the robot system is the ability of tracking the predefined trajectory. First we analyze the trajectory tracking in the presence of external forces/torques, which are considered as disturbance. For the torque controlled part we use the controller defined by Eq. (10). Combining Eqs. (10) and (2) together and considering external torques τ_{ext_t} acting on the torque controlled joints yields:

$$\left[\hat{\mathbf{H}}_{vt}(\mathbf{q}) \quad \hat{\mathbf{H}}_t(\mathbf{q})\right]\begin{bmatrix}\ddot{\mathbf{q}}_{v_c}\\ \ddot{\mathbf{q}}_{t_c}\end{bmatrix}+\left[\hat{\mathbf{C}}_{tv}(\dot{\mathbf{q}},\mathbf{q}) \quad \hat{\mathbf{C}}_t(\dot{\mathbf{q}},\mathbf{q})\right]\begin{bmatrix}\dot{\mathbf{q}}_v\\ \dot{\mathbf{q}}_t\end{bmatrix}+\hat{\mathbf{g}}_t(\mathbf{q})=$$

$$=\left[\mathbf{H}_{vt}(\mathbf{q}) \quad \mathbf{H}_t(\mathbf{q})\right]\begin{bmatrix}\ddot{\mathbf{q}}_v\\ \ddot{\mathbf{q}}_t\end{bmatrix}+\left[\mathbf{C}_{tv}(\dot{\mathbf{q}},\mathbf{q}) \quad \mathbf{C}_t(\dot{\mathbf{q}},\mathbf{q})\right]\begin{bmatrix}\dot{\mathbf{q}}_v\\ \dot{\mathbf{q}}_t\end{bmatrix}+\mathbf{g}_t(\mathbf{q})+\tau_{ext_t}.$$

Assuming that there is no error in the dynamic model of the system i.e. $(\hat{\cdot})=(\cdot)$ and that the velocity controlled subsystem assures good tracking of the trajectory reference $\ddot{q}_{v_c}=\ddot{q}_v$ yields

$$\mathbf{H}_t\ddot{\mathbf{q}}_{t_c}=\mathbf{H}_t\ddot{\mathbf{q}}_t+\tau_{ext_t}. \tag{11}$$

Task space analysis

Starting from Eq. (11) both sides of equation are premultiplied by $\mathbf{H}_t^{-1}$ and by $\mathbf{J}_t$. Let $\mathbf{J}_t$ be the right part of the Jacobian matrix $\mathbf{J}$ associated with the torque controlled subsystem and $\mathbf{J}_v$ the left part of Jacobian matrix associated with the velocity controlled subsystem, $\mathbf{J}=[\mathbf{J}_v\,|\,\mathbf{J}_t]$. Then, by premultiplying (11) by $\mathbf{J}_t\mathbf{H}_t^{-1}$ yields

$$\mathbf{J}_t \ddot{\mathbf{q}}_{t_c} = \mathbf{J}_t \ddot{\mathbf{q}}_t + \mathbf{J}_t \mathbf{H}_t^{-1} \tau_{ext_t}. \tag{12}$$

Then, by add in the term $\mathbf{J}_v \ddot{\mathbf{q}}_{v_c}$ and after simplification yields

$$\mathbf{J}\ddot{\mathbf{q}}_c = \mathbf{J}\ddot{\mathbf{q}} + \mathbf{J}_t \mathbf{H}_t^{-1} \tau_{ext_t}. \tag{13}$$

Substituting Eq. (4) for $\ddot{\mathbf{q}}_c$ and using $\mathbf{J}\mathbf{J}^{\#} = \mathbf{I}$, $\mathbf{J}\mathbf{N} = 0$ and $\ddot{\mathbf{x}} = \mathbf{J}\ddot{\mathbf{q}} + \dot{\mathbf{J}}\dot{\mathbf{q}}$ and then using Eq. (7) we derive the final equation that describes dynamics of the error in the task space:

$$\ddot{e} + \mathbf{K}_d \dot{e} + \mathbf{K}_p e = \mathbf{J}_t \mathbf{H}_t^{-1} \tau_{ext_t}. \tag{14}$$

The dynamics of the error is also a function of the robot configuration $\mathbf{q}$, since $\mathbf{J}_t$ and $\mathbf{H}_t$ are functions of the configuration.

3.1.1 Null space analysis

Starting from the same equation as in the previous case (11) and premultiplying it by $\mathbf{H}_t^{-1}$ and $\mathbf{N}_t$. $\mathbf{N}_t$ is right part of the matrix $\mathbf{N}$ that is associated with the torque controlled subsystem and $\mathbf{N}_v$ is left part of the matrix $\mathbf{N}$ that is associated with the velocity controlled subsystem $\mathbf{N} = [\mathbf{N}_v \,|\, \mathbf{N}_t]$. It yields

$$\mathbf{N}_t \ddot{\mathbf{q}}_{t_c} = \mathbf{N}_t \ddot{\mathbf{q}}_t + \mathbf{N}_t \mathbf{H}_t^{-1} \tau_{ext_t},$$

then we add the term $\mathbf{N}_v \ddot{\mathbf{q}}_{v_c}$ and simplify to

$$\mathbf{N}\ddot{\mathbf{q}}_c = \mathbf{N}\ddot{\mathbf{q}} + \mathbf{N}_t \mathbf{H}_t^{-1} \tau_{ext_t}. \tag{15}$$

Again substituting Eq. (4) for $\ddot{\mathbf{q}}_c$ and using $\mathbf{N}\mathbf{J}^{\#} = 0$, $\mathbf{N}\mathbf{N} = \mathbf{N}$ and $\ddot{\mathbf{q}} = \mathbf{J}^{\#}(\ddot{\mathbf{x}} - \dot{\mathbf{J}}\dot{\mathbf{q}}) + \mathbf{N}\ddot{\mathbf{q}}$ and using Eq. (8) we derive the final equation that describes dynamics of the error in the null space:

$$\mathbf{N}(\ddot{e}_n + \mathbf{K}_n \dot{e}_n) = \mathbf{N}_t \mathbf{H}_t^{-1} \tau_{ext_t}. \tag{16}$$

Using Lyapunov stability theory we can define stability region of the controller parameters. Let us select Lyapunov function

$$v = \frac{1}{2} \dot{e}_n^T \mathbf{W} \dot{e}_n$$

and it follows

$$\dot{v} = \dot{e}_n^T \mathbf{W} \ddot{e}_n + \frac{1}{2} \dot{e}_n^T \dot{\mathbf{W}} \dot{e}_n =$$

$$= -\dot{e}_n^T \mathbf{W}\mathbf{N}\mathbf{K}_n \dot{e}_n + \dot{e}_n^T \mathbf{W}\mathbf{N}_t \mathbf{H}_t^{-1} \tau_{ext_t} + \frac{1}{2} \dot{e}_n^T \dot{\mathbf{W}} \dot{e}_n =$$

$$= -\dot{e}_n^T (\mathbf{W}\mathbf{K}_n - \frac{1}{2} \dot{\mathbf{W}}) \dot{e}_n + \dot{e}_n^T \mathbf{W}\mathbf{N}_t \mathbf{H}_t^{-1} \tau_{ext_t}, \tag{17}$$

since $\dot{e}_n^T = \dot{e}_n^T \mathbf{N}^T$ and $\mathbf{N}^T\mathbf{W} = \mathbf{W}\mathbf{N}$. If the above requirement ensures negative definiteness of $\dot{v}$ the system is asymptotically stable. Therefore, the system without the external forces ($\tau_{ext_t} = 0$) is asymptotically stable if the matrix is $\mathbf{W}\mathbf{K}_n - \frac{1}{2}\dot{\mathbf{W}}$ is positive definite. This means that to low value of the parameter $\mathbf{K}_n$ destabilize the system (Nemec [1997]).

3.2 External force analysis

3.2.1 Forces acting on the robot end-effector

The external force that acts on the robot end-effector $\mathbf{F}_0$ produces the torques in all robot joints. Since the velocity controller is stiff to the external forces, the forces do not affect the motion of the velocity controlled subsystem. On the other hand the torques in the torque controlled subsystem affect the motion and have to be analyzed. Torques in the joints of the torque controlled subsystem are defined as:

$$\tau_{ext_t} = \mathbf{J}_t^T \mathbf{F}_0. \tag{18}$$

Using Eq. (14) the following nonhomogenous differential equation is derived

$$\ddot{e} + \mathbf{K}_d \dot{e} + \mathbf{K}_p e = \mathbf{J}_t \mathbf{H}_t^{-1} \mathbf{J}_t^T \mathbf{F}_0. \tag{19}$$

The equation describes the dynamics of the error in the task space in presence of the external force acting on the robot end-effector.

Žlajpah (Žlajpah [1997]) has shown that the system is stable for bounded external force $\mathbf{F}_0$ and that error $\ddot{e}$ converges to some limited region.

When setting the controller parameters $\mathbf{K}_p$ and $\mathbf{K}_d$ we have to consider task space error dynamics (14) and also a desired response to an external force (19). Higher value of the parameter $\mathbf{K}_p$ makes the the system stiffer to external force and faster when tracking the trajectory. On the other hand to large value of the $\mathbf{K}_p$ causes oscillation of the system and can cause instability of the real system, because real system often has time delays and death zones in the controller loop. Higher values of the $\mathbf{K}_d$ increases damping to the external force and slows down the response, but improves the stability of the system.

3.2.2 Dynamic consistency

The system is dynamically consistent when torques in the null space do not produce any accelerations in the task space (Khatib [1995]) and when forces in the task space do not produce any accelerations in the null space (Nemec and Žlajpah [2002]). According to Khatib (Khatib [1995]) the system is dynamically consistent only when inertia weighted generalized inverse is used. Using inertia matrix as weight the kinetic energy of the system is also minimized (Hollerbach [1987]). On the other hand the generalized inverse weight can be any symmetric positive definite matrix of size $n \times n$ (Nakamura [1991]), where n is the number of DOF of the system. Depending on the weight different criterion can be fulfilled. For example, joint velocities of the

system can be minimized or the error of the secondary task can be decreased (Lenarčič [2000]) etc.
Using the inertia weighted inverse the dynamic consistency can be achieved only for the torque controlled robot systems. In contrary, in case of combined controlled systems the dynamic consistency can not be achieved using inertia weighted generalized inverse. In this section we will analyze the influence of the external force on the null space motion and the possibility of the dynamic consistency.
The external force produces torques in robot joints which can affect the null space motion. Using the equations (16) and (18) yields

$$\mathbf{N}(\ddot{e}_n + \mathbf{K}_n \dot{e}_n) = \mathbf{N}_t \mathbf{H}_t^{-1} \mathbf{J}_t^T \mathbf{F}_0.$$

The system is dynamically consistent if the external force $\mathbf{F}_0$ does not affect the null space motion, yielding

$$\mathbf{N}_t \mathbf{H}_t^{-1} \mathbf{J}_t^T = 0. \tag{20}$$

Let us define a selection matrix $\mathbf{I}_t$

$$\mathbf{I}_t = \begin{bmatrix} \mathbf{0} \\ \mathbf{I} \end{bmatrix}.$$

The lower part of the matrix is the identity matrix $\mathbf{I}$ of the size equal to the number of DOF of the torque controlled system and upper part is the corresponding zero matrix. If we choose the weighting matrix as:

$$\mathbf{W}^{-1} = \mathbf{I}_t \mathbf{H}_t^{-1} \mathbf{I}_t^T \tag{21}$$

and using relations $\mathbf{J}_t = \mathbf{J}\mathbf{I}_t$ and $\mathbf{N}_t = \mathbf{N}\mathbf{I}_t$ it can be easily shown that using selected weight Eq. (20) is fulfilled. So, using the weight (21) the external force $\mathbf{F}_0$ does not produce any null space accelerations, and consequently, the system is dynamically consistent.
We could easily see that using selected weight both subsystems are separated, which is not desired.

3.2.3 Forces acting on the robot segments

An external force acting on the robot segments causes torques directly in the null space independent on the generalized inverse weight. The force acting on the torque controlled part moves the segments away from the force, i.e. a robot is compliant in the null space. Consequently, the retreat produces the null space tracking error (16).
The controller gain $\mathbf{K}_n$ in Eq. (8) defines the compliance of the robot to the external force. However, the compliance depends also on the robot configuration and its inertia matrix (16). Higher value of $\mathbf{K}_n$ enables better trajectory tracking in the null space and the robot is stiffer to the external force in the null space. In contrast, lower value of $\mathbf{K}_n$ makes the robot more compliant in the null space and the trajectory tracking is worsened.
We will show later that high compliance in the null space assures obstacle avoidance. For that, low values of $\mathbf{K}_n$ are necessary, which can make the system unstable, i.e. the derivative of the Lyapunov function (17) becomes positive definite.

Note that the external force acting on the robot segments influences also the task space motion and causes the task space error as shown in Eq. (14). Of course, when the external force vanishes the task space error converges to zero.

3.2.4 The force acting on the velocity controlled subsystem

On the other hand, the robot is not compliant to an external force acting on the velocity controlled part. The external force produces only torques in the velocity controlled joints, since the velocity controlled system is first in the kinematic chain. Because the velocity controller is stiff and assures tracking of the trajectory, the external force does not affect the motion of the system.

4. Verification of combined control by simulation

In this section we compare three different approaches to the robot control: a velocity control, a torque control and the proposed combined control. We have made the comparison on a model of a real robot system composed of a torque controlled planar manipulator mounted on a velocity controlled holonomic platform (Fig. 1).
Note that the comparison is only a raw comparison of different approaches, since there exists numerous variants of velocity and torque control. Although, the comparison is good and fair enough to see some basic properties of combined control.

4.1 Controller definitions

First controller is a velocity controller, where the entire system is controlled by a velocity. Each joint is controlled by a PID controller with optimal parameters that assures good joint trajectory tracking. We used the following velocity controller:

$$\dot{\mathbf{q}}_c = \mathbf{J}^{\#}\left(\dot{\mathbf{x}}_r + \mathbf{K}_p e\right) + \mathbf{N}\dot{\varphi}. \tag{23}$$

Second case is a torque controller, where the entire system is torque controlled. We used a resolved acceleration control:

$$\tau_c = \hat{\mathbf{H}}(\mathbf{q})\ddot{\mathbf{q}}_c + \hat{\mathbf{C}}(\dot{\mathbf{q}},\mathbf{q})\dot{\mathbf{q}} + \hat{\mathbf{g}}(\mathbf{q}). \tag{24}$$

The third compared controller is the proposed combined controller.
Controller parameters of all three cases are optimal and were defined in such a way that all three systems have similar responses to some reference trajectory (see next section).

4.2 Trajectory tracking

First we analyze the tracking of the end-effector trajectory. The desired trajectory is a circle with radius 1 m. Two different periods was used. For slower motion the period was 1 s and for the faster motion it was 0.1 s.
Fig. 3 and Fig. 4 show the tracking error of all three controllers. For slower motion the tracking errors are approximately the same, because the controller parameters were set for such motion. Here, the motion is slow. Therefore, dynamic interactions between different joints are small and all three controllers assure good trajectory tracking.

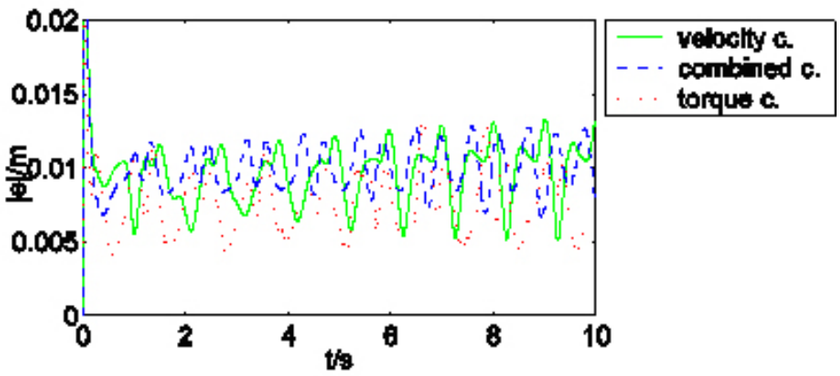

Fig. 3. Task space error in case of slower circular trajectory

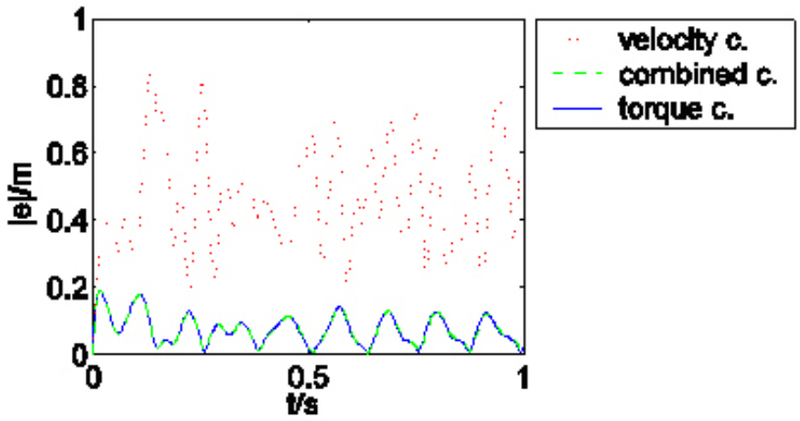

Fig. 4. Task space error in case of faster circular trajectory.

On the other hand, for the faster motion (Fig. 4) the dynamic interactions between joints are larger. Therefore, the tracking error of the velocity controller is much higher than in the case of other two controllers, since the velocity controller does not consider any dynamic interactions. The torque controller considers all dynamic interactions and the combined controller considers all the influence on the manipulator and none on the platform (10). In our case the weight of the platform is significantly higher as the weight of the manipulator and the influence on the platform is low.

4.3 Force acting on the robot end-effector

When the robot end-effector is in contact with the environment a contact force appears. None of the three controllers controls the force directly and none considers this force in the control algorithm. Therefore, the external force in all three controllers is considered as a disturbance.

The contact with the environment occurs when a part of the trajectory is inside of an object. In our experiment the trajectory reference was 5 cm inside of the object in x direction. The stiffness of the object was 5000 N/m. The initial configuration of the robot is shown in Fig. 7. This figure shows the top view of the mobile manipulator. Large circle corresponds to the platform. On top of the platform is the manipulator marked with strait lines. Next figures show the error in task space (Fig. 5) and the force on the end-effector (Fig. 6), which results from the contact.

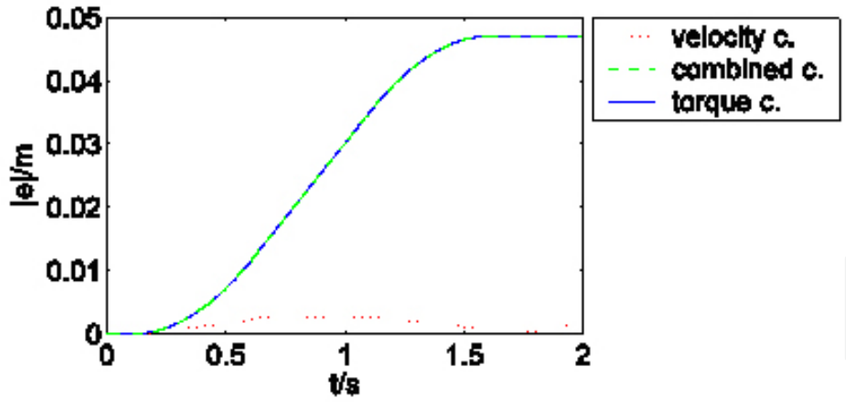

Fig. 5. Error in the task space.

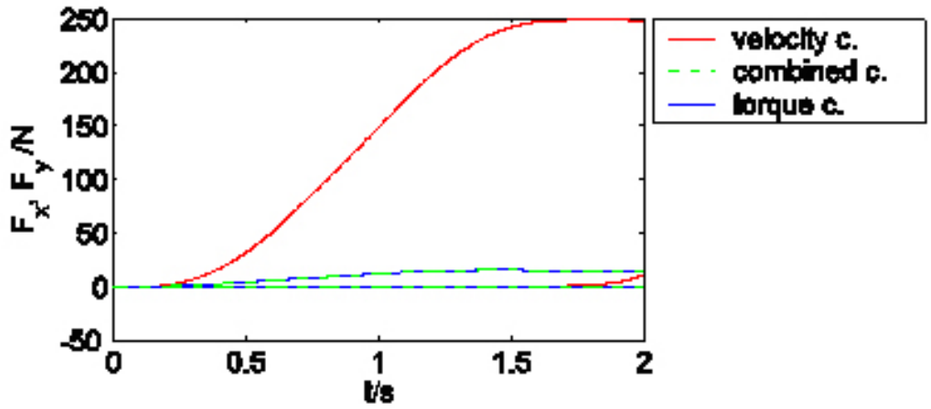

Fig. 6. Force on the end-effector.

The velocity controlled system is usually very stiff to external force, as can be seen in the figures. The error is small, and consequently the force of the contact is large, since the end-effector is "deep" in the object. The stiffness of the system is defined by internal joint velocity controllers that usually have large gains in order to achieve good tracking performance despite disturbances.

In the case of torque controlled system an external force produces torques in the joints. If the system is not dynamically consistent, i.e. the weight is not the inertia matrix, the external force affects the motion in the null space. This often leads to singular configuration of the manipulator. Hence, the dynamic consistency is preferred. Here, the torques in the joints resulting from the external force are completely compensated by the control torques.

Responses of the torque controlled dynamically compensated system are shown in the Fig. 5 and Fig. 6. The external force is significantly lower than with the velocity controller, since the torque controlled system is more compliant to external forces and consequently, task space error is higher. The compliance depends on the controller parameters and the robot configuration. The parameters were set in such a way that high compliance is achieved.

In the case of combined control the response of the system is similar as in the case of the torque controller. Here, the dynamic consistency is not feasible due to a facts described in the section 0. However, using the inertia matrix as a weight, the properties of the system can be quite similar to a dynamically consistent system. The self motion is very low due to the large weight corresponding to the platform and is noticeable after longer time.

4.4 Forces acting on the mobile manipulator segments

4.4.1 Forces acting on the manipulator

In our experiment we apply a force of 10 N on the end of 2-nd segment of the manipulator as shown in Fig. 7.

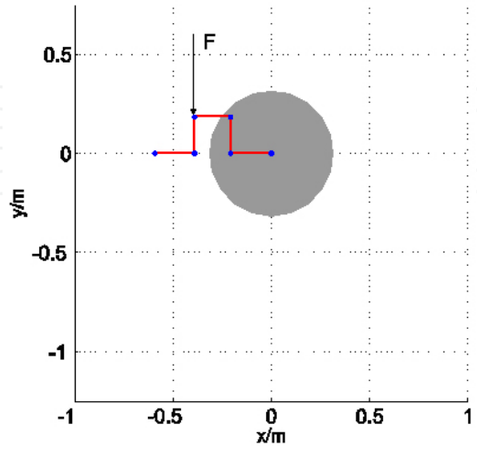

Fig. 7. The external force acting on the manipulator.

In the case of velocity controlled system the external force did not cause any noticeable configuration changes (Fig. 8). Consequently, the task space error was low (Fig. 11). As already mentioned, the velocity controlled system is stiff to an external force, regardless of where a force acts.

In the case of combined controller the external force causes a displacement of the manipulator in the point of the contact (Fig. 9 a)). Consequently, the task space error appears (Fig. 11) and the platform moves in order to decrease the task space error. The configuration after 100 s of acting the force is shown in Fig. 9 b). The platform has moved up and therefore part of the manipulator between point of the contact and a base or end-effector is singular and the manipulator is no more compliant to the external force (for details see Žlajpah [1999]).

We achieve best results with the torque controlled system. The external force causes a displacement of the entire system (including the platform) (Fig. 10). The task space error is approximately the same as with the combined control (Fig. 11).

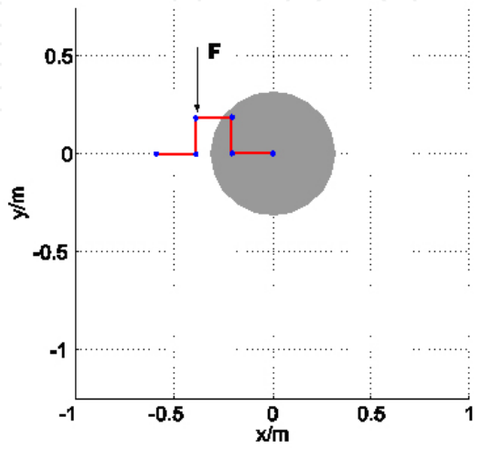

Fig. 8. Configuration of the robot after 2 s of acting the force (velocity control)

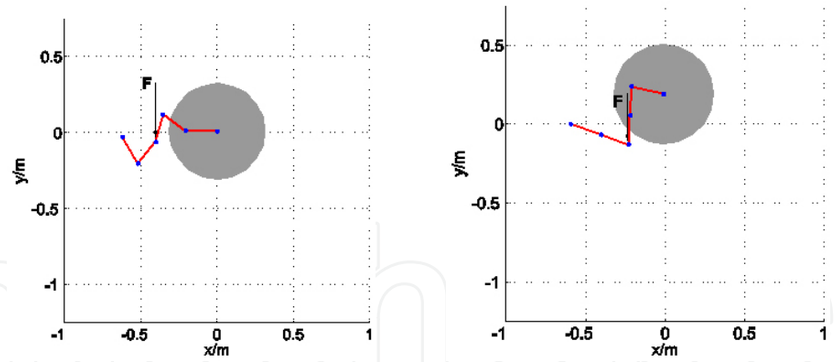

a) After 2 s of acting the force b) After 100 s of acting the force

Fig. 9. Configuration of the robot after acting the force (combined control).

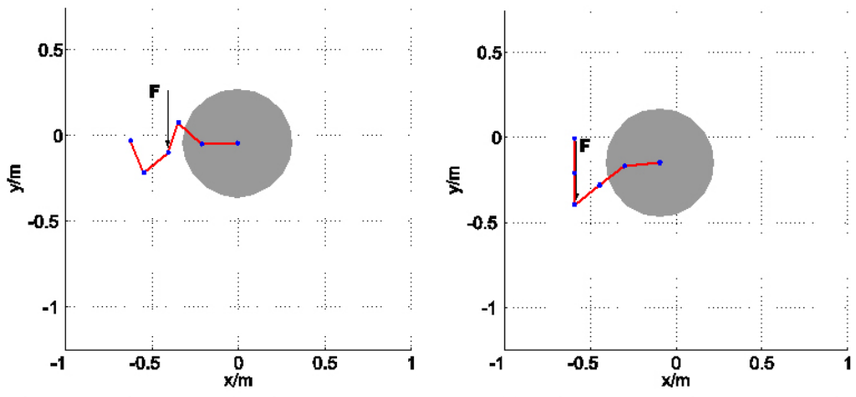

a) After 2 s of acting the force b) After 100 s of acting the force

Fig. 10. Configuration of the robot after acting the force (torque control).

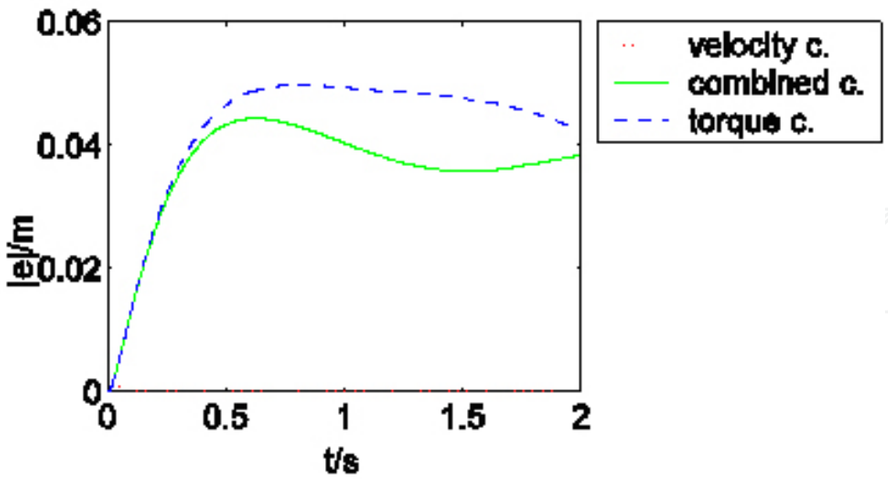

Fig. 11. Task space error.

4.4.2 Forces acting on the platform

We applied a force of 10 N on the platform as shown in Fig. 12. In this case the largest disadvantage of the combined control can be seen. Responses of the velocity and the combined controlled systems are the same, since in both cases the velocity controller assures

stiff response of the platform to an external force acting on the platform. The configuration remains the same in both cases despite of the external force (Fig. 12). The task space error is negligible (Fig. 14).

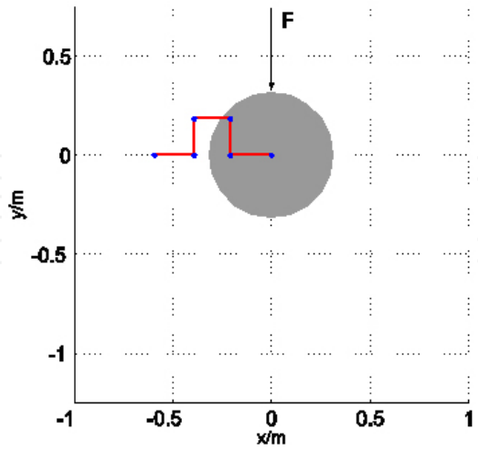

Fig. 12. Point of acting the force on the platform.

In the case of the torque controller the platform moves in the direction away from the force (Fig. 13), similar as the manipulator moved in the previous case. The task space error is consequently higher (Fig. 14).

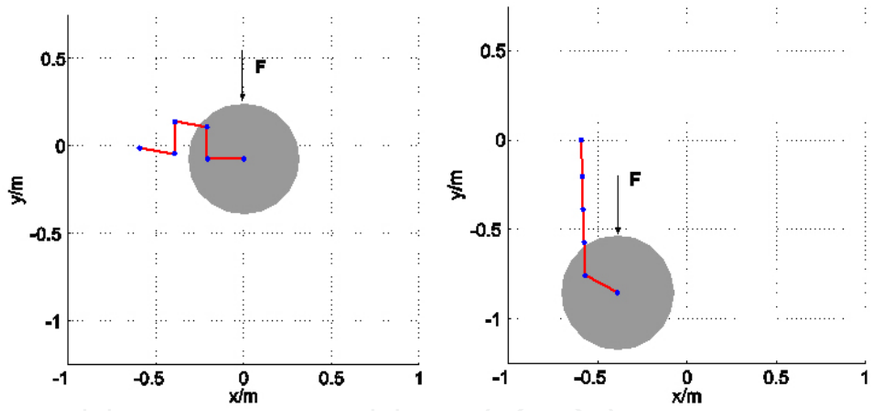

a) After 2 s of acting the force b) After 100 s of acting the force

Fig. 13. Configuration of the robot after acting the force on the platform (torque control).

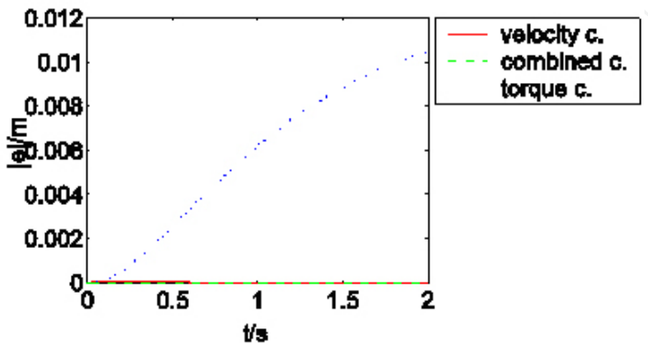

Fig. 14. Task space error.

5. Experiments on real system

5.1.1 Determination of the generalized inverse weight

The drawback of the proposed approach is that the system is not dynamically consistent although using inertia weighted generalized inverse. When using the inertia weighted generalized inverse the kinetic energy of the system is minimized. However, the minimization of the kinetic energy is not desired in our case. Namely, the platform is much heavier (150 kg) than the segments of the manipulator (50 g to 900 g). Because of this large difference in weights, the kinetic energy minimization results in motion, where most of the motion is done by the manipulator. Consequently, the manipulator often comes into singular configuration (manipulator stretches), while the platform is practically not moving. To avoid this problem, we propose to change the generalized inverse weight matrix as follows:

$$\mathbf{W} = \begin{bmatrix} \mathbf{H}_v(\mathbf{q}) & \mathbf{H}_{tv}(\mathbf{q}) \\ \mathbf{H}_{vt}(\mathbf{q}) & k * \mathbf{H}_t(\mathbf{q}) \end{bmatrix}. \tag{17}$$

The value of the parameter k affects only the part corresponding to the kinetic energy of the manipulator used in the minimization. In our case the value of the k was defined empirically and set to 10.

5.2 The task of the mobile manipulator

In our case the mobile manipulator is supposed to move in unknown environment with unknown moving obstacles. The primary task is to track a prescribed end-effector trajectory and the secondary task is the obstacle avoidance.

5.2.1 Obstacle avoidance

For obstacle avoidance certain information of the environment is needed. Many commercially available mobile platforms already have integrated sonar sensors for detection of obstacles around the platform. Based on the proximity measurements the platform is moved away from the obstacles. Like most of the local strategies that solve the obstacle avoidance at the kinematic level, the approach we use is to assign each point, which is close to an obstacle, a motion component in a direction away from the obstacle. The repulsive velocity in the null space corresponding to the translational velocities of the platform $\dot{\mathbf{q}}_{n_{xy}}$ can be defined as:

$$\dot{\mathbf{q}}_{n_{xy}} = \begin{cases} -\sum_i w_i K_s \left(\frac{d_{soi}}{\|d_{0_i}\|} - 1 \right) \frac{d_{0_i}}{\|d_{0_i}\|}, & \forall d_{0_i} < d_{soi} \\ 0, & else \end{cases}.$$

All obstacles inside the sphere of influence are included in the repulsive velocity. If only the closest obstacle is included in the repulsive velocity the switching between two or more obstacles could occur and consequently, the discontinuity in the repulsive velocity.

Unlike in the case of mobile platforms, robot manipulators usually do not possess integrated sensors for obstacle detection in 3D space. In the past, there were some attempts to integrate some kind of "sensitive skin" and similar sensors along the robot manipulator links (Lumelsky, Siemens tactile sensors, ...), but this solution is very complicated and not suitable for practical applications. Perhaps the most promising are the laser sensors and the 3D vision. As an alternative we propose an approach, where obstacles are actually not avoided,

but the contact forces, which occur after the collision between the manipulator links and obstacles, are minimized. The minimization of contact forces is done by a compliant control of a manipulator in the null space (Eq.(16)). For details see (Omrčen et al. [2004]). The same principle can be noticed by humans working in dark environments.
To achieve obstacle avoidance by compliant control the manipulator has to be torque controlled and back-drivable [Žlajpah [1998]], i.e. any external force at the manipulator is immediately felt at the motors of the manipulator.

5.3 Implementation on a real system

The proposed algorithm was implemented on a mobile manipulator and the results were compared to the results of a manipulator with a fixed base controlled only by the torque. The mobile manipulator used in our experiments was described in section 0 and is shown in Fig. 1. The primary task was trajectory tracking. The secondary task was the obstacle avoidance for the platform. The system was compliant in null space and stiff in the task space. We used $\mathbf{K}_p = 1000$, $\mathbf{K}_v = 160$, $\mathbf{K}_n = 1$ for the controller gains. First we show the comparison between undisturbed motion of the mobile manipulator and the fixed manipulator. Later the mobile manipulator motion in space with obstacles and in contact with the environment is shown.

5.4 Free motion

The motion of both systems in the free space is shown. Two different trajectories were tested. The first was a circle with a radius 15 cm and a period of 20 s and the second was a larger circle with a radius 50 cm and a period of 50 s.
Fig. 15 a.) and Fig. 16 a.) show the trajectory of the end effector in (x-y) plane and b.) show the tracking error of the fixed and mobile manipulator, respectively. The average integral absolute error (AIAE) is defined as:

$$AIAE = \frac{1}{t_{final}} \int_0^{t_{final}} \sqrt{e_x^2 + e_y^2}\, dt, \tag{20}$$

where e_x and e_y are the tracking error in x and y direction, respectively. The AIAE of the fixed manipulator was 7.5 mm and of mobile manipulator was 8.5 mm. The accuracy of the mobile manipulator was slightly smaller.

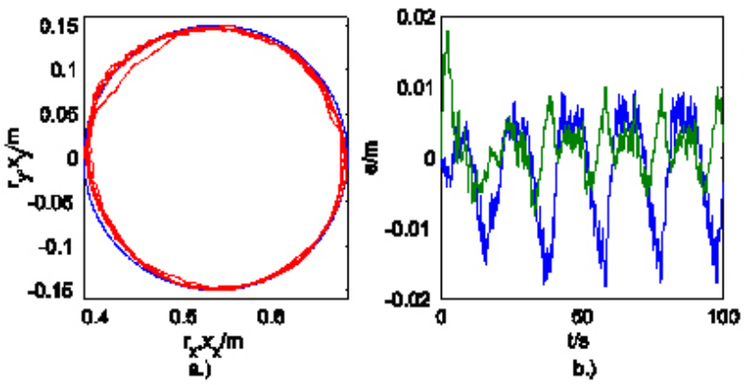

Fig. 15. Undisturbed motion of the fixed manipulator (circle r=15 cm). a.) trajectory, b.)tracking error.

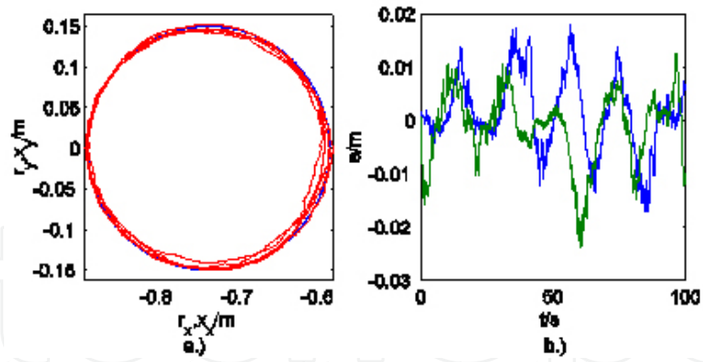

Fig. 16. Undisturbed motion of the mobile manipulator (circle r=15 cm). a.) trajectory, b.)tracking error.

The added mobility makes the workspace of the manipulator larger which can be seen when tracking the larger circle. Fig. 17 shows the motion of the fixed manipulator before reaching the end of its workspace, after that point the tracking error started to increase. With added mobility the workspace is infinite. The mobile manipulator tracked the whole trajectory, in spite of tracking the larger circle (Fig. 18). The AIAE of the larger circle was 7.5 mm and was approximately the same as the AIAE of the smaller circle.

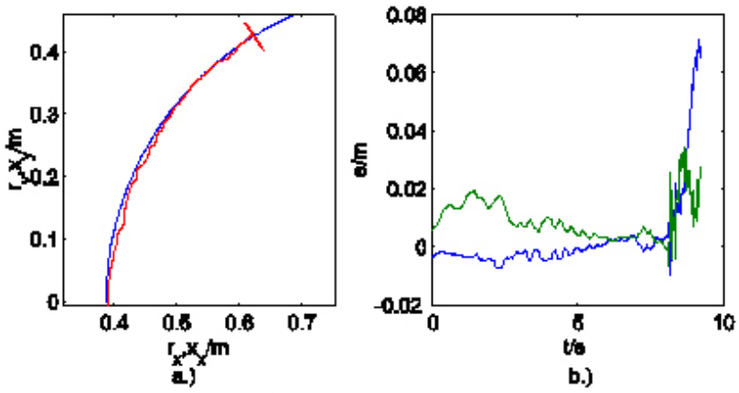

Fig. 17. Undisturbed motion of the fixed manipulator (circle r=50 cm). The manipulator came in the singularity and the motion is stopped. a.) trajectory, b.)tracking error.

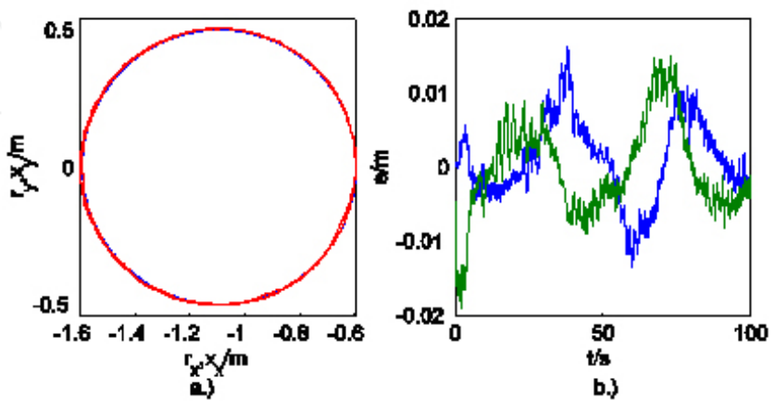

Fig. 18. Undisturbed motion of the mobile manipulator (circle r=50 cm). a.) trajectory, b.)tracking error.

5.5 Motion in unstructured space

The mobile manipulator moved in space with obstacles. The obstacles close to the platform were detected with the ultrasonic sensors. There were also obstacles that collided with the manipulator and were not detected. The trajectory reference was the larger circle.

When the manipulator avoided the obstacles using the action-reaction principle the AIAE was 6.9 mm. When only the obstacles near the platform were present the AIAE was 8.6 mm. In case when obstacles near the platform and manipulator affected the motion the AIAE was 8.0 mm. Fig. 19 shows the motion when all obstacles was present. In this case the platform motion was much larger than in free motion case (Fig. 20). The AIAEs were approximately same as in undisturbed case. The maximal tracking error was larger when the obstacles collided the manipulator because the contact force affects the task space error. But after the contact the error decreased and the AIAE was approximately the same.

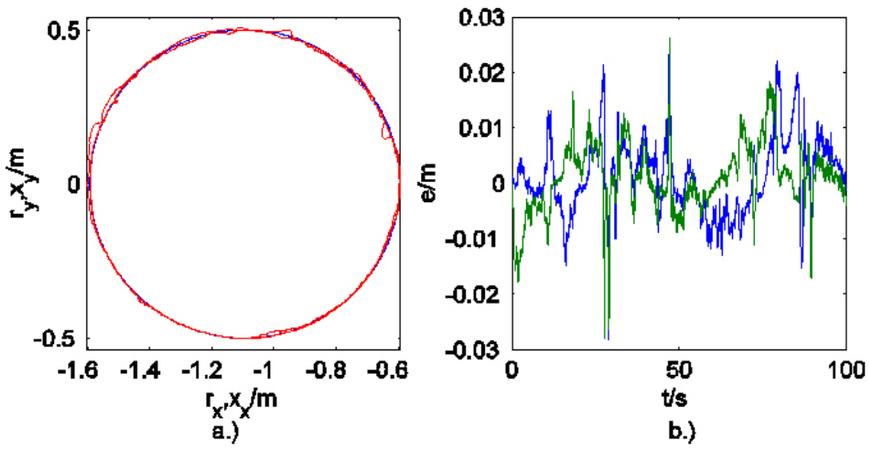

Fig. 19. Motion of the mobile manipulator in space with obstacles (circle r=50 cm).

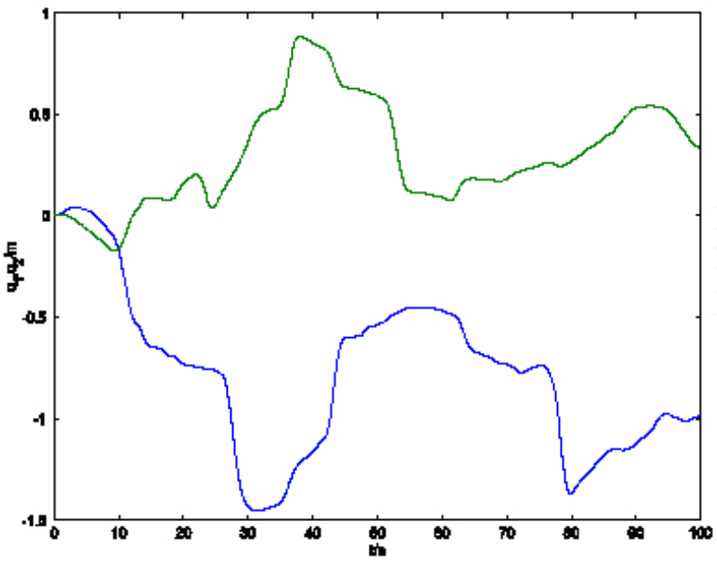

Fig. 20. Motion of the platform. The cause for this motion was mostly obstacle repulsion.

Fig. 21 shows the top view of the configuration of the mobile manipulator before and after the collision with the obstacle. The large blank circle shows the trajectory and

the smaller circles show obstacles detected with ultrasonic sensors. F denotes the force of the obstacle that collides with the platform. The collision place is only approximate because the obstacle position and force were not measured. The manipulator moved away from the obstacle after the collision in 0.8 s. The impact force was approximately 4 N.

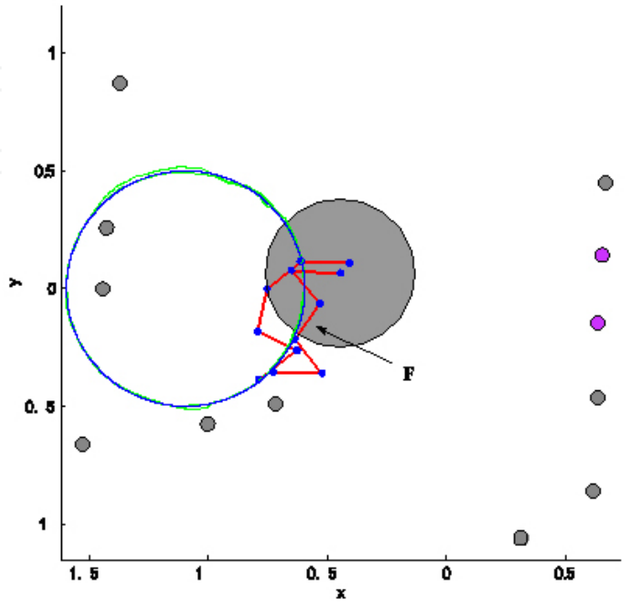

Fig. 21. Configuration of the mobile manipulator before and after the collision.

5.6 Motion in contact with the environment

One part of the trajectory reference (large circle) was inside of the wall. The mobile manipulator end-effector was tracking the trajectory to the wall and than it was pressing to the wall. The force of the contact is not controlled directly. It is dependent on the tracking error and the manipulator configuration. The motion of the manipulator in contact is shown in Fig. 22. Fig. 23 shows the force on the wall. Force measurement was used only for validation and not for the control.

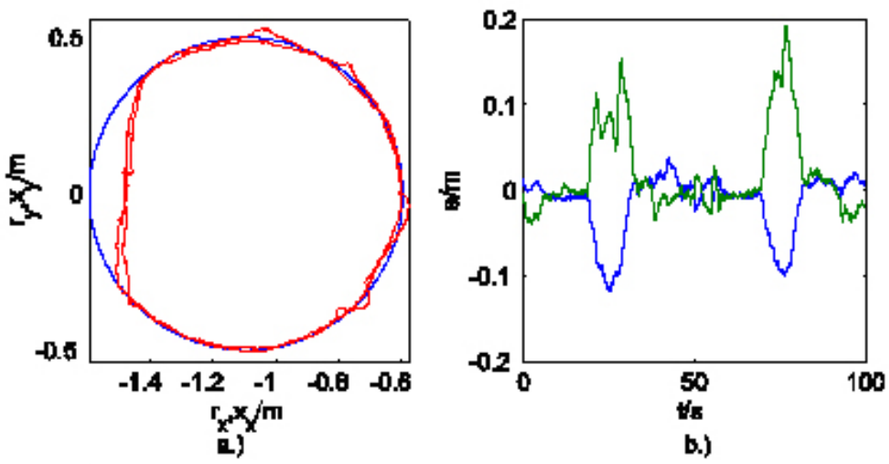

Fig. 22. Motion of the mobile manipulator in space with obstacles in contact with the wall.

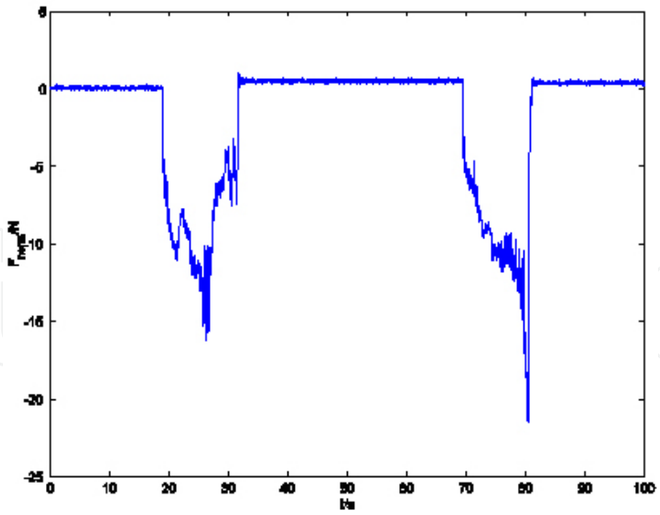

Fig. 23. Normal component of the manipulator force on the wall.

6. Conclusion

The use of the robots in the real world mostly depends on the development of a autonomous robotic systems that integrate mobility and manipulability. This chapter has presented a new approach to the robot control. The control is called combined control since it combines (integrates) two different types of robot control, i.e. the torque and the velocity control in a single robot system. Later on the mathematical analysis of the proposed combined control has been shown. Verification has been done on a simulated and a real system composed of a velocity controlled mobile platform and a torque controlled manipulator.

The results show good tracking of the desired trajectory in the task space and in the null space depending on the controller gains. Controller gains also define the compliance of the system in the task and in the null space. We defined the stability region of controller gains.

Regarding the system performance the combined control can be placed somewhere between velocity and torque control. Most of the properties of the combined control are comparable to those of the torque control and they are much better than those of the velocity control. When considering the trajectory tracking the combined control is comparable to the torque control, since in both cases most of dynamic interactions are compensated. The disadvantage of the combined control is inability of dynamic consistency and stiff behavior of the system when external forces act on the velocity controlled subsystem. On the other hand, the system with the combined controller can be compliant to external forces acting on the end-effector or on the segments of the torque controlled subsystem.

We have proved on a real system that the compliant control enables the mobile manipulator to avoid all obstacles in its workspace. Some of the obstacles are detected and they generate repulsive velocity. On the other hand we do not detect obstacles near the manipulator; avoidance is obtained by compliant control in the null space. We achieved a compliancy also in the task space.

Summarizing, the combined control is suitable for most applications where torque control is desired and part of the system can not be torque controlled. Additionally, no hardware modification of the motor controller in velocity controlled subsystem is necessary.

7. References

C. Altafini. Inverse kinematic along a geometric spline for a holonomic mobile manipulator. In International Conference on Robotics and Automation, pages 1265-1270, Seoul, 2001.

H. Asada and J.-J. E. Slotine. Robot Analysis and Control. A Wiley Interscience publication, John Wiley and Sons, Inc., 1986.

N. Hogan. Impedance control: an approach to manipulation. ASMe J. Dynamic System, Meas. and Control, 107:1-24, 1985.

J. M. Hollerbach. Redundancy resolution of manipulators through torque optimization. Journal of Robotics and Automation, 3(4):308-316, 1987.

R. Holmberg and O. Khatib. Development and control of a holonomic mobile robot for mobile manipulation tasks. The International Journal of Robotics Research, 19(11):1066-1074, 2000.

P. Hsu, J. Hauser, and S. Sastry. Dynamic control of redundant manipulators. Journal of Robotic Systems, 6(2):133-148, 1989.

O. Khatib. Mobile manipulation: The robotic assistant. Robotics and Autonomous Systems, 26:175-183, 1999.

O. Khatib. Inertial properies in robotic manipulation: An object-level framework. International Journal of Robotic Research, 14(1):19-36, 1995.

J. Lenarčič. On the execution of the secondary task of redundant manipulators. Robotics and Autonomous Systems, 30:231-236, 2000.

J. Luh, M. Walker, and R. Paul. Resolved-acceleration control of mechanical manipulators. IEEE Transactions on Automatic Control, 25(3):468- 474, 1980.

Y. Nakamura. Advanced Robotics: Redundancy and Optimization. Addison-Wesley Publishing Company, Inc., 1991.

B. Nemec. Force control of redundant robots. In 5-th IFAC Symposium on Robot Control, Nantes, France, 1997.

B. Nemec and L. Žlajpah. Force control of redundant robots in unstructured environments. IEEE Trans. on Industrial Electronics, 49(1):233-240, 2002.

D. Oetomo, M. Ang Jr., R. Jamisola, and O. Khatib. Integration of torque controlled arm with velocity controlled base for mobile manipulation: An application to aircraft canopy polishing. In Fourteenth CISM-IFToMM Symposium on Robotics RoManSy, pages 308-317, Udine, Italy, 2002.

D. Omrčen. Kombinacija hitrostnega in navornega vodenja pri mobilnem robotskem manipulatorju. Založba FE in FRI, Ljubljana, PhD disertaion, 2005.

D. Omrčen and J. Lenarčič. Vodenje redundantnega sistema mobilne platforme z manipulatorjem. In Electrotechnical and Computer Science Conference (ERK 2001), volume B, pages 425-426, Portoro^{o}, Slovenija, 2001.

D. Omrčen, L. Žlajpah, and B. Nemec. Autonomous motion of a mobile manipulator using a combined torque and velocity control. Robotica, 22 (6):623-632, 2004.

R. S. Oropeza and M. Devy. Motion control using visual servoing and potential fields for a rover-mounted manipulator. In International Conference on Robotics and Automation, pages 233-240, Detroit, Michigan, 1999.

L. Petersson, D. Austin, and D. Kragic. High-level control of a mobile manipulator for door opening. In IEEE/RSJ International Conference on Intelligent Robots and Systems, volume 3, pages 2333-2338, Takamatsu, Kagawa, Japan, 2000.

M.H. Raibert and J.J. Craig. Hybrid position/force control of manipulators. Journal of Dynamic Systems, Measurement and Control, 102:126-133, 1981.

J. Salisbury. Active stiffness control of a manipulator in cartesian coordinates. In Proceedings of the 19th IEEE Int. Conference on Decision and Control, pages 95-100, Albuquerque, New Mexico, USA, 1980.

Y. Yamamoto and X. Yun. Effect of the dynamic interaction on coordinated control of mobile manipulators. IEEE Transactions on Robotics and Automation, 12(5):816-824, 1996.

L. Žlajpah. Influence of external forces on the behaviour of redundant manipulators. Robotica, 17:283-292, 1999.

L. Žlajpah. Compliant motion control of redundant manipulators in constraint space. In Fifth IFAC Symposium on Robot Control (SYROCO'97), pages 657-663, Nantes, France, 1997.

L. Žlajpah. Obstacle avoidance control for redundant manipulators utilizing the contact forces. In IEEE International Conference on Intelligent Engineering Systems, pages 343-348, Vienna, Austria, 1998.

Mobile Robotics, Moving Intelligence

Edited by Jonas Buchli

ISBN 3-86611-284-X

Hard cover, 586 pages

Publisher Pro Literatur Verlag, Germany / ARS, Austria

Published online 01, December, 2006

Published in print edition December, 2006

This book covers many aspects of the exciting research in mobile robotics. It deals with different aspects of the control problem, especially also under uncertainty and faults. Mechanical design issues are discussed along with new sensor and actuator concepts. Games like soccer are a good example which comprise many of the aforementioned challenges in a single comprehensive and in the same time entertaining framework. Thus, the book comprises contributions dealing with aspects of the Robotcup competition. The reader will get a feel how the problems cover virtually all engineering disciplines ranging from theoretical research to very application specific work. In addition interesting problems for physics and mathematics arises out of such research. We hope this book will be an inspiring source of knowledge and ideas, stimulating further research in this exciting field. The promises and possible benefits of such efforts are manifold, they range from new transportation systems, intelligent cars to flexible assistants in factories and construction sites, over service robot which assist and support us in daily live, all the way to the possibility for efficient help for impaired and advances in prosthetics.

How to reference

In order to correctly reference this scholarly work, feel free to copy and paste the following:

Damir Omrcen, Leon Zlajpah and Bojan Nemec (2006). Combined Torque and Velocity Control of a Redundant Robot System, Mobile Robotics, Moving Intelligence, Jonas Buchli (Ed.), ISBN: 3-86611-284-X, InTech, Available from: http://www.intechopen.com/books/mobile_robotics_moving_intelligence/combined_torque_and_velocity_control_of_a_redundant_robot_system

InTech Europe
University Campus STeP Ri
Slavka Krautzeka 83/A
51000 Rijeka, Croatia
Phone: +385 (51) 770 447
Fax: +385 (51) 686 166
www.intechopen.com

InTech China
Unit 405, Office Block, Hotel Equatorial Shanghai
No.65, Yan An Road (West), Shanghai, 200040, China
中国上海市延安西路65号上海国际贵都大饭店办公楼405单元
Phone: +86-21-62489820
Fax: +86-21-62489821

IntechOpen